RSC Advances

PAPER

View Article Online
View Journal | View Issue

Cite this: *RSC Adv.*, 2022, **12**, 22097

$ZnO–ZnCr_2O_4$ composite prepared by a glycine nitrate process method and applied for hydrogen production by steam reforming of methanol

Chung-Lun Yu,[a] Subramanian Sakthinathan,[a] Guan-Ting Lai,[a] Chia-Cheng Lin,[a] Te-Wei Chiu *[a] and Ming-Che Liu*[bc]

To address climate change, the energy crisis, and global warming, hydrogen (H_2) can be used as a potential energy carrier because it is clean, non-toxic and efficient. Today, the mainstream industrial method of H_2 generation is steam reforming of methanol (SRM). In this process, a zinc-based commercial catalyst is usually used. In this work, a $ZnO–ZnCr_2O_4$ catalyst was successfully synthesised by the glycine nitrate process (GNP) and developed for use in H_2 production by SRM. The specific surface area, porous structure and reaction sites of the zinc-based catalyst were effectively increased by the preparation method. The as-combusted $ZnO–ZnCr_2O_4$ composite catalyst had a highly porous structure due to the gas released during the GNP reaction process. Moreover, according to the ZnO distribution and different G/N ratios, the specific surface area (S_{BET}) of the as-combusted $ZnO–ZnCr_2O_4$ catalyst varied from 29 $m^2\ g^{-1}$ to 46 $m^2\ g^{-1}$. The $ZnO–ZnCr_2O_4$ composite catalyst (G/N 1.7) exhibited the highest hydrogen production, 4814 ml STP min^{-1} g-cat^{-1}, at a reaction temperature of 450 °C without activation treatment. After activation, the $ZnO–ZnCr_2O_4$ composite catalyst achieved hydrogen production of 6299 ml STP min^{-1} g-cat^{-1} at a reaction temperature of 500 °C. The hydrogen production performance of the $ZnO–ZnCr_2O_4$ composite powder was improved by the uniform addition of ZnO to $ZnCr_2O_4$. Based on the performance, this $ZnO–ZnCr_2O_4$ composite catalyst has great potential to have industrial and economic impact due to its high efficiency in hydrogen production.

Received 31st May 2022
Accepted 1st August 2022

DOI: 10.1039/d2ra03383f

rsc.li/rsc-advances

1. Introduction

Because of environmental issues such as global warming, fossil energy use, and the energy crisis, hydrogen (H_2) energy has attracted the attention of industrial and scientific communities. Moreover, hydrogen energy is clean and harmless to the environment.[1–3] The nature and characteristics of hydrogen energy make it a possible replacement for fossil energy. Hence, hydrogen fuel cells are viewed as a possible energy source for the automotive field because of their stable operation, low cost, and carbon-free nature. Fuel cell-based chemical reactions to directly generate electricity also have the advantages of low pollution and high efficiency.[1]

For the growth of a hydrogen energy economy, the challenges of the effective production, storage, and transport of hydrogen need to be met.[4] Therefore, the progress of the popularization of fuel cell vehicles (FCV) in each country is directly affected by the hydrogen infrastructure, such as the cost and challenges of hydrogen storage, hydrogen transport, and leakage.[5] The risk of flammability is high when the hydrogen concentration in air is between 4% and 75%. This range is wider than that of natural gas, which is between 5% and 15%. Given the risks, the safety of hydrogen storage techniques is important to society.[6–8] Most hydrogen storage media use metal hydrides, but such system storage capacity is insufficient.[9–11] To solve these challenges, hydrogen generation from a steam reforming system uses various conversion sources.[12–14]

When methanol and water vapor react in the presence of a suitable catalyst, they can produce H_2 and CO. For H_2 conversion, methanol offers advantages over other resources such as methane, gasoline, and ethanol.[15] Due to the lowest ratio of hydrogen to carbon from the methanol chemical formula, carbon emissions are lower than those of other liquid hydrogen conversion sources, leading to less carbide production.[16,17] Especially, because methanol has no C–C bond, the amount of coke fabricated in SRM is lower. The operation is safe, and the sulfur compound content is low (<5 ppm). For these reasons, SRM is the worthiest method for high-efficiency hydrogen production.[18]

[a]*Department of Materials and Mineral Resources Engineering, National Taipei University of Technology, 1, Sec. 3, Zhongxiao E. Rd, Taipei, 106, Taiwan. E-mail: tewei@ntut.edu.tw*

[b]*Clinical Research Center, Taipei Medical University Hospital, Taipei 11031, Taiwan. E-mail: d204097002@tmu.edu.tw*

[c]*School of Dental Technology, College of Oral Medicine, Taipei Medical University, Taipei 11031, Taiwan*

The general reaction processes that produce hydrogen from methanol are mainly divided into three forms: (1) thermal decomposition, (2) partial oxidation, and (3) steam reforming.[19,20] However, they have important differences. The decomposition reaction has obvious and strong endothermic phenomena, and CO is produced as a byproduct. Hence, the decomposition reaction is not desirable in fuel cells.[21,22] Partial oxidation has a strong exothermic reaction, and if pure oxygen is replaced with air, the hydrogen production rate is 66%.[23] In contrast, the endothermic process of steam reforming allows efficient hydrogen production.[24] The by-product is CO, and the hydrogen production rate can reach 75%. Among the various methods, steam reforming of methanol has miscibility with water, a low reforming temperature (250 °C), and a low CO production rate, so it is preferred by industry for efficient hydrogen production.[17]

$$CH_3OH \rightarrow CO + 2H_2,\ \Delta H_0 = 128\ kJ\ mol^{-1} \quad (1)$$

$$CH_3OH + 1/2O_2 \rightarrow CO_2 + 2H_2,\ \Delta H_0 = -155\ kJ\ mol^{-1} \quad (2)$$

$$CH_3OH + H_2O \rightarrow CO_2 + 3H_2,\ \Delta H_0 = 131\ kJ\ mol^{-1} \quad (3)$$

In the SRM process, hydrogen is generally produced from methanol in three ways: (4) water gas shift (WGS), (5) decomposition of methanol, and (6) methanol steam reforming, as shown below.[25]

$$CH_3OH + H_2O \rightarrow CO_2 + 3H_2 \quad (4)$$

$$CH_3OH \rightarrow CO + 2H_2 \quad (5)$$

$$CO + H_2O \rightarrow CO_2 + H_2 \quad (6)$$

SRM is a simple and effective process to produce hydrogen due to the endothermic process during the reaction, so it is suitable for fuel cell applications. Moreover, the equipment of SRM requires no hydrogen storage station because of the gas existing. For the preparation of the metal-based composite catalysts used in SRM, elements with highly active elements, such as Zn, Cu, Ru, and Pd, are used. The various elements and reaction conditions have significant effects on performance. According to previous research, Cu-based catalysts produce outstanding results in various applications, especially in the hydrogen production reaction conditions, due to their lower reaction temperature and high sensitivity. Hence, Cu-based catalysts have good potential as materials and have received much interest in industry. However, when a Cu-based catalyst reacts at over 350 °C, the catalytic efficiency and life cycle decrease because the copper ions are easily over-reduced and crystallize into metallic copper particles, thereby losing the active sites. Furthermore, the deposition of carbon particles throughout the SRM process is the primary cause of decreased catalytic activity.[26–28] To extend the cycle-life and increase efficiency, different metal oxides, such as ZnO,[29–32] ZrO_2,[33,34] Al_2O_3,[35] Ga_2O_3,[36] Fe_2O_3,[37] and CeO_2,[38–40] can be incorporated to improve the function of the catalyst. Meanwhile, the perovskite oxides catalyst was expected as a potential material that was employed for thermochemical fuel production.[41–43] With proper methods for modifying the existing catalyst, the Cu-based catalyst has better the thermal stability, efficiency, and dispersion after the incorporation of the metal oxide in the Cu-based catalyst.

The glycine nitrate process (GNP), which is synthesis procedure, was proposed in 1967 by Professor A. G. Merzhanov.[44] This GNP synthesis technique uses the heat released by chemical reactions to promote synthesis, and it has been applied in several fields, such as flat plates and lithium batteries.[45] Meanwhile, the grain size can also affect the catalytic function. A special characteristic of GNP is that it can create a fluffy structure due to the gas produced in the reaction and restrain grain growth.[8,46] In the SRM process, Cu-based catalysts have high activity, but they also have the disadvantage of high sensitivity to the reaction environment.[47] Given the disadvantages of Cu-based catalysts, challenges still exist to their application. These challenges include long-term performance retention, stability under extreme reaction environments, and narrow reaction temperature range for optimal hydrogen production. Therefore, suitable alternatives need to be developed for the SRM process.[29]

Zinc–chromium (Zn–Cr) oxide has long been used as a catalyst to generate methanol under high temperature and pressure. The good performance exhibited by Zn–Cr oxide is due to its crystallization during high-temperature steam reforming. Zn–Cr oxide can maintain high activity and high stability.[48] Zn–Cr based spinel oxide exhibits high function in applications such as CO and C_xH_y oxidation,[49] alcohol generation,[50] removals of organic contaminants,[51] and isobutanol synthesis.[48] However, higher thermal treatments could deactivate the Zn–Cr catalyst and degrade its stability. According to Liu *et al.*, the stable spinel structure can prevent a high drop in pressure, which otherwise could damage a vehicle.[52] $ZnCr_2O_4$ has been used as a catalyst and demonstrated high thermal stability and mechanical stability.[53] Furthermore, $ZnCr_2O_4$ also has high activity and good photocatalytic performance.[54] Katte *et al.* revealed the synergistic effect of Cu and ZnO in promoting methanol production.[55] To avoid the drawbacks of higher sintering temperatures, the synergetic effect of contact between ZnO and $ZnCr_2O_4$ increases the catalytic function because of the strong attachment of the two phases.[48] In this project, the ZnO–$ZnCr_2O_4$ composite catalyst was made by the GNP method and applied to hydrogen generation by SRM. Moreover, the porous structure of the catalyst was increased by the GNP method, as compared to that resulting from the traditional solid-state reaction, and improved the function of the ZnO–$ZnCr_2O_4$ composite catalyst in hydrogen production.

2. Experiment procedure

2.1 Materials and methods

The starting reagents, namely, zinc nitrate hexahydrate [$Zn(NO_3)_2 \cdot 6H_2O$], glycine [$C_2H_5NO_2$], and chromium nitrate nonahydrate [$Cr(NO_3)_3 \cdot 9H_2O$] were purchased from SHOWA and Sigma-Aldrich. The as-combusted catalyst in this study was investigated by suitable instrumentation techniques. The

crystalline structures of the ZnO–$ZnCr_2O_4$ composite catalyst and $ZnCr_2O_4$ catalyst were analyzed by X-ray diffractometric (D2 Phaser, Bruker) with a working voltage of 30 kV under Cu $K\alpha$ radiation. The morphology and particle size of the as-combusted catalyst in this study were studied by field emission scanning electron microscopy (JEOL FE-SEM. JSM-7610F). The specific surface area (S_{BET}) was measured by Brunauer–Emmett–Teller (BET) method with a Gemini V Micromeritics, Surface Area, and Pore Size Analyzer. A suitable amount of prepared catalyst was degassed at 200 °C for 24 hours and the absorbed water was removed by passing high purity N_2 through the catalyst before BET measurement. N_2 adsorption isotherms were measured and investigated at various relative pressures (P/P_0) of 0 to 0.3 while the catalyst adsorbed N_2.

2.2 Preparation of ZnO–$ZnCr_2O_4$ composite and $ZnCr_2O_4$ catalysts

ZnO–$ZnCr_2O_4$ and $ZnCr_2O_4$ catalysts were prepared by as-combusted GNP method.[56] The molar ratios of zinc nitrate to glycine were 1 : 1.5 and 1 : 1.7, and the two catalysts were referred to as G/N-1.5 and G/N-1.7, respectively. Zinc nitrate to chromium nitrate molar ratios were 1 : 1 and 1 : 2 for the fabrication of the ZnO–$ZnCr_2O_4$ composite and $ZnCr_2O_4$. All starting reagents were dissolved in 80 ml DI water and stirred at 80 °C for 12 hours. After that, the precursor solution was dried in an oven at 100 °C for 48 hours to evaporate the remaining water until the precursor is gel-like. The obtained solution was heated on a hotplate and spontaneously combusted at approximately 300 °C. The reaction yielded gray powder and NO_2 gas.[57]

2.3 Catalyst test

The as-combusted Zn-based catalysts were placed in a tubular reactor. The carrier gas used in the process was N_2 with a flow rate of 30 sccm and a quartz tube inner diameter of 1.2 cm. A flowchart of the SRM process is presented in Fig. 1. The gas product converted in the process was analyzed and measured several times at each reaction temperature with a GC-1000 gas chromatograph equipped with a thermal conductivity detector and the resulting values were averaged. Before the catalysts were testing, all of the specific samples with and without activation by flow reactor received pre-oxidation treatment by annealing in a mixture of gas of 10% H_2 and 90% N_2 at 650 °C for 1 hour. For every experiment, 0.02 g of catalyst was put into a quartz tube. A gas chromatograph (GC 1000 Chromatography with TCD) with

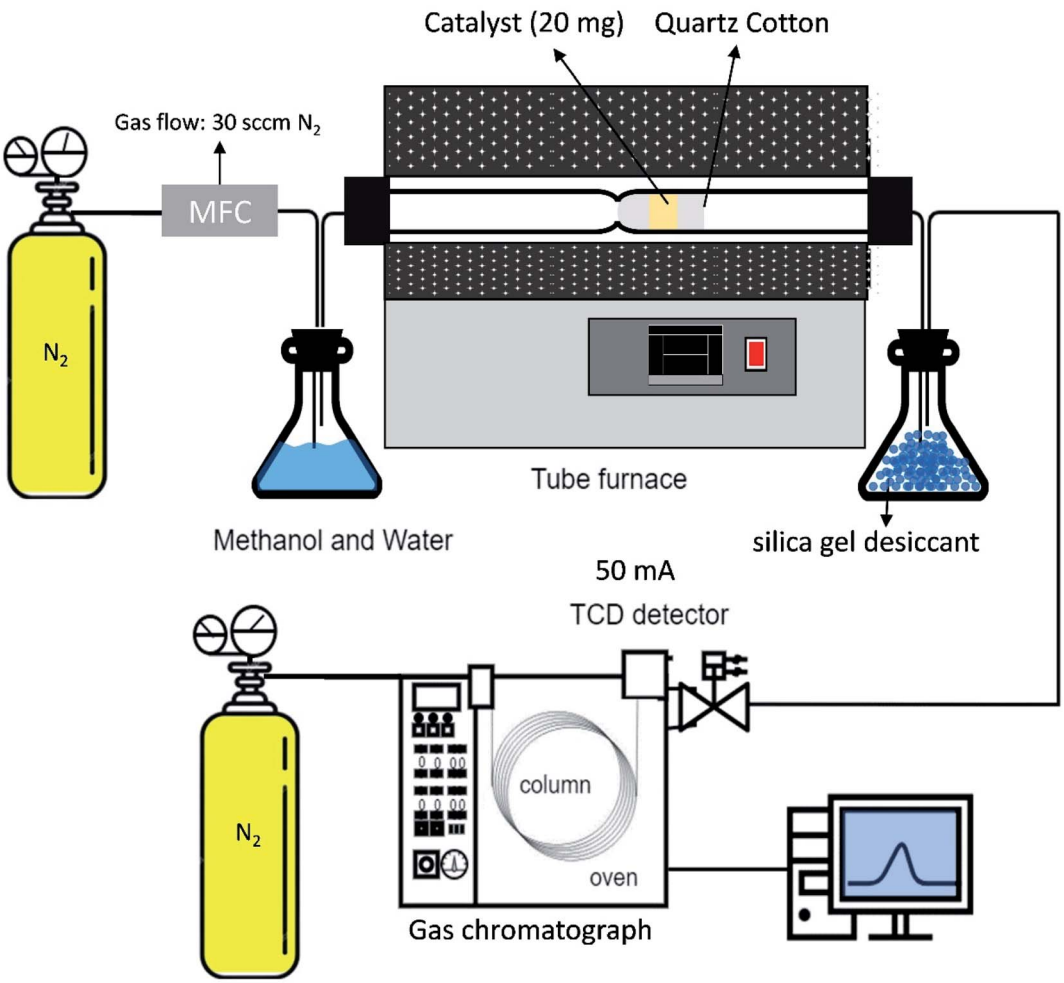

Fig. 1 Flowchart diagram of the methanol steam reforming process.

one column (60/80 Carboxen® 1000) for H_2 (7 ft 1/16 in, stainless steel) was used to measure the hydrogen production. In the gas chromatograph, a thermal conductivity detector with a current of 50 mA was fitted. The H_2 production performances of the ZnO–$ZnCr_2O_4$ and $ZnCr_2O_4$ catalysts were investigated based on the H_2 production rate from the gas chromatograph.[58,59]

$$\text{Methanol conversion } (\%) = \frac{(\text{methanol})\text{in} - (\text{methanol})\text{out}}{(\text{methanol})\text{in}} \times 100 \quad (7)$$

$$\text{Hydrogen production rate} = \frac{H_2\%\cdot\text{mL}\cdot 30\ \text{mL min}^{-1}}{\text{cm}^3\cdot\text{g}} \quad (8)$$

3. Results and discussion

3.1 Characteristics of ZnO–$ZnCr_2O_4$ composite catalyst and $ZnCr_2O_4$ catalyst prepared by GNP

XRD studies of the as-combusted catalysts were performed with the database software Powder-XRD. Fig. 2(a–d) reveal the XRD patterns of as-combusted $ZnCr_2O_4$ (GNP: 1.5, 1.7) and ZnO–$ZnCr_2O_4$ (GNP: 1.5, 1.7). The XRD curves in Fig. 2(a) and (b) reveal the diffraction patterns of $ZnCr_2O_4$ prepared with G/N ratios of 1.5 and 1.7. The diffraction spectra of the cubic phase spinel $ZnCr_2O_4$ (PDF# 87-0028) showed diffractions at 30.3°, 35.7°, 43.4°, 53.8°, 57.4° and 63.1°, which corresponded to the (220), (311), (400), (422), (511) and (400) planes. On the other hand, the diffraction pattern of the ZnO phase in Fig. 2(c) was based on the increasing metal source ratio of zinc nitrate to chromium nitrate. Furthermore, Fig. 2(d) shows that the intensity of the ZnO diffraction peak decreased due to the decrease in the G/N ratio because the conditions were insufficient for the ZnO phase to crystallize. Meanwhile, the ZnO–$ZnCr_2O_4$ synthesized with a lower G/N ratio, the reaction temperature would decrease, and the diffraction peaks became broader which revealed the crystallite of the ZnO–$ZnCr_2O_4$ was smaller. The diffraction patterns of hexagonal phase ZnO (PDF# 79-0206) are shown in Fig. 2(c). The peaks at 31.7°, 34.4°, and 36.2° corresponded to the (100), (002) and (101) planes. Based on the XRD patterns of as-combusted $ZnCr_2O_4$ (GNP: 1.5, 1.7) and ZnO–$ZnCr_2O_4$ (GNP: 1.5, 1.7), immiscibility of ZnO and $ZnCr_2O_4$ was judged by the non-shift XRD peak from the ZnO–$ZnCr_2O_4$, and no other secondary phases such as Cr_2O_3 and $ZnCrO_4$ were observed in the pattern.

Moreover, the activated catalysts were respectively investigated for their characterization. Fig. 3 showed the XRD patterns of catalysts after activation. Fig. 3(a) $ZnCr_2O_4$ catalyst prepared by the GNP method with G/N ratios 1.7 revealed the phase remained $ZnCr_2O_4$ spinel phase and Fig. 3(b) ZnO–$ZnCr_2O_4$ catalyst prepared by the GNP method with G/N ratios 1.7 revealed the $ZnCr_2O_4$ spinel phase and slightly ZnO hexagonal phase, respectively.

The microscopic surface morphologies and the structures of the as-combusted catalysts were analyzed by FESEM. Fig. 4 presents FESEM images of (a) $ZnCr_2O_4$ prepared by the GNP method with a G/N ratio of 1.7, (b) $ZnCr_2O_4$ prepared by the GNP method with a G/N ratio of 1.5, (c) ZnO–$ZnCr_2O_4$ prepared by the GNP method with a G/N ratio of 1.7, and (d) ZnO–$ZnCr_2O_4$ prepared by the GNP method with a G/N ratio of 1.5 before the SRM treatment. The as-combusted $ZnCr_2O_4$ presented a coral-

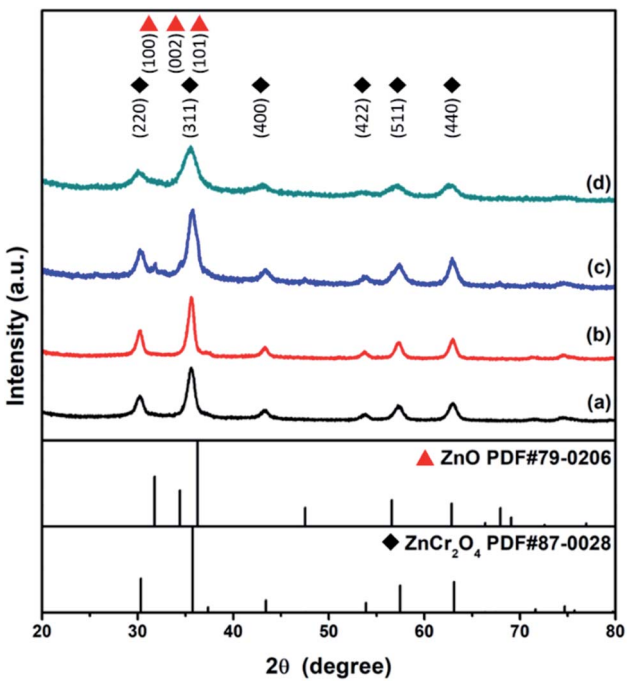

Fig. 2 XRD patterns of $ZnCr_2O_4$ catalysts prepared by the GNP method with G/N ratios of (a) 1.7 and (b) 1.5, and ZnO–$ZnCr_2O_4$ catalyst synthesis by the GNP method with G/N ratios of (c) 1.7 and (d) 1.5.

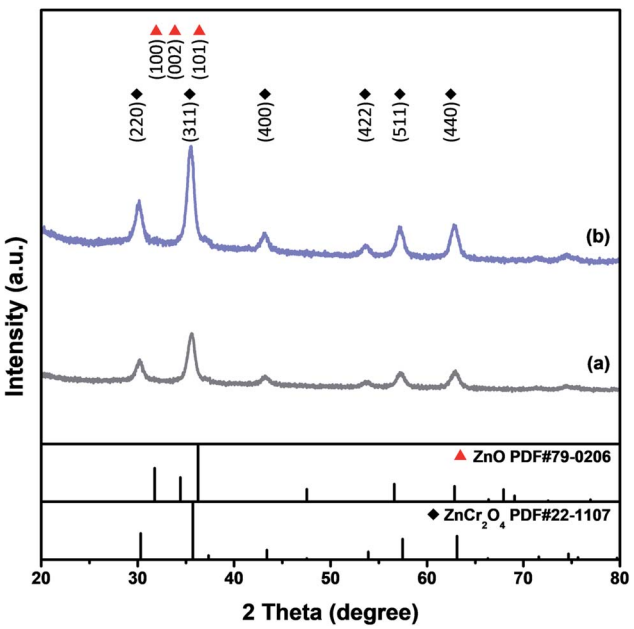

Fig. 3 XRD patterns of activated (a) $ZnCr_2O_4$ and (b) ZnO–$ZnCr_2O_4$ catalyst prepared by the GNP method with G/N ratios 1.7.

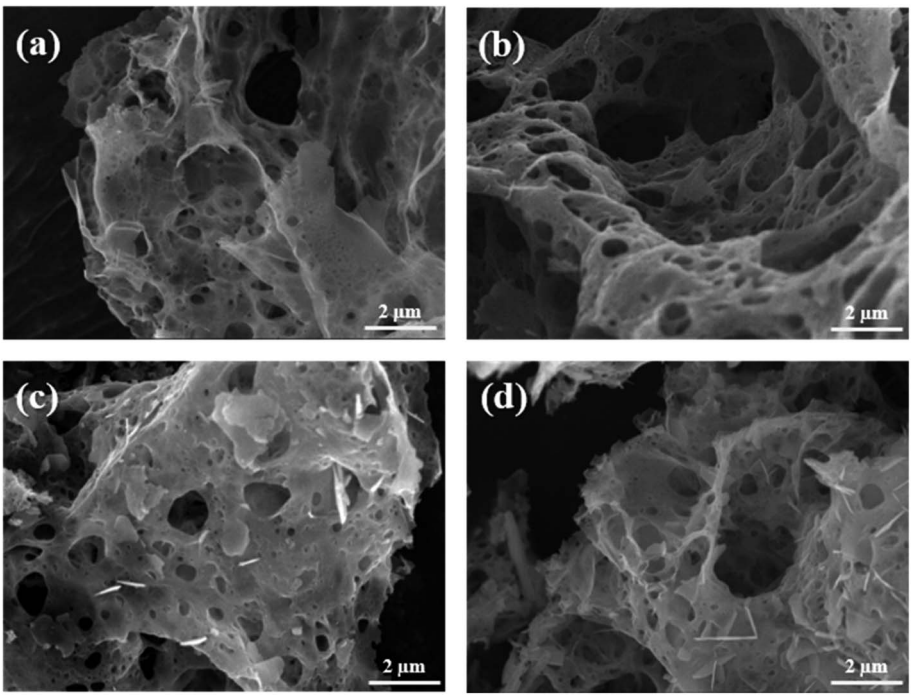

Fig. 4 SEM images of $ZnCr_2O_4$ catalysts prepared by the GNP method with G/N ratios of (a) 1.7 and (b) 1.5, and ZnO–$ZnCr_2O_4$ catalysts prepared by the GNP method with G/N ratios of (c) 1.7 and (d) 1.5.

like porous structure due to the gas that was released during the reaction. However, the hexagonal flakes attached to the porous structure in Fig. 4(c) and (d) were ZnO, corresponding to the XRD result in Fig. 2. Based on the XRD and SEM analysis the of as-combusted catalysts, the ZnO was in the amorphous phase in the ZnO–$ZnCr_2O_4$ during the GNP when the G/N ratio was 1.5. Moreover, the as-combusted catalyst after activation still retains the porous structure which was shown in Fig. 5. However, compared to Fig. 4 and 5, the pore on the catalyst and the ZnO attached on the catalyst surface was shown to be smaller. Thus, it is exhibited that agglomeration occurs after activation.

The specific surface areas of the as-combusted ZnO–$ZnCr_2O_4$ and $ZnCr_2O_4$ catalysts prepared by GNP (with G/N ratios of 1.5 and 1.7) are listed in Table 1. Before BET analysis, the remaining absorbed water was removed from the catalysts by high purity N_2 flow at 200 °C for 24 hours. N_2 adsorption isotherms were investigated at various relative pressures while the catalyst adsorbed N_2. A high specific surface area would facilitate the

Table 1 The specific surface areas of ZnO–$ZnCr_2O_4$ and $ZnCr_2O_4$ catalysts prepared by GNP and the activated ZnO–$ZnCr_2O_4$ and $ZnCr_2O_4$ catalysts

	Specific surface area (m^2 g^{-1})	
Composition	Original catalyst	Activated catalyst
$ZnCr_2O_4$ G/N-1.7	29	27
$ZnCr_2O_4$ G/N-1.5	46	—
ZnO–$ZnCr_2O_4$ G/N-1.7	35	48
ZnO–$ZnCr_2O_4$ G/N-1.5	45	—

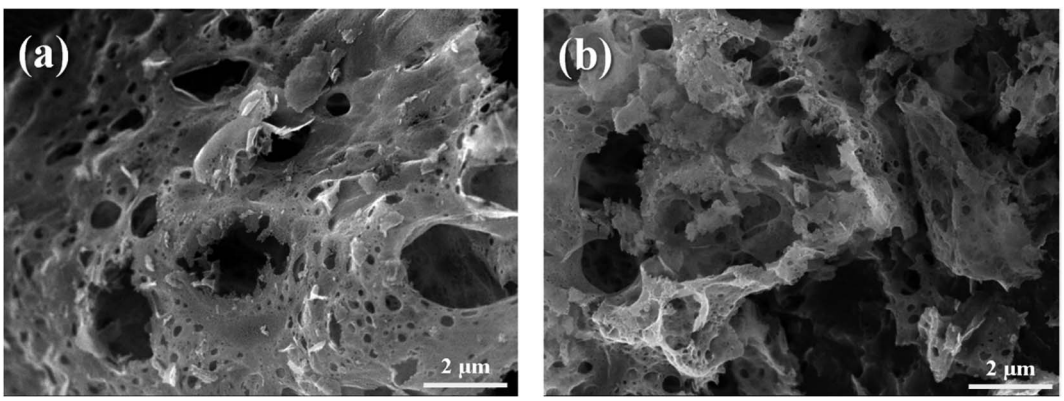

Fig. 5 SEM images of activated (a) $ZnCr_2O_4$ and (b) ZnO–$ZnCr_2O_4$ catalyst prepared by the GNP method with G/N ratios 1.7.

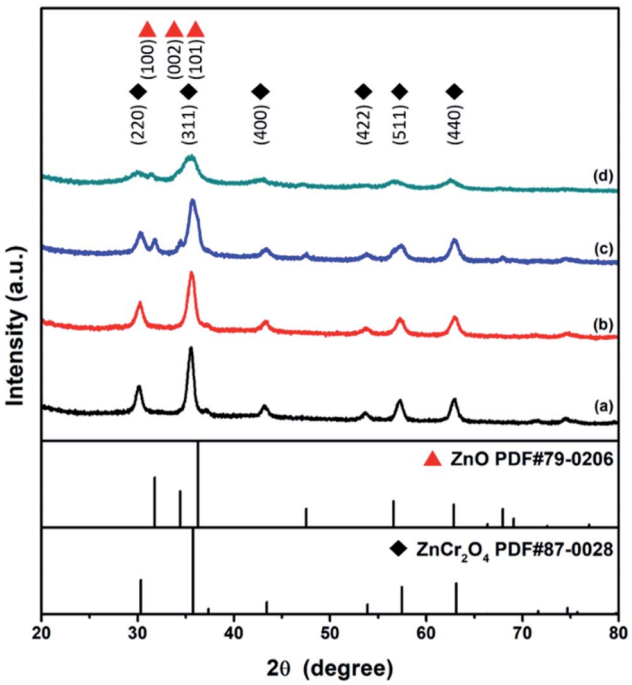

Fig. 6 XRD patterns of $ZnCr_2O_4$ catalysts prepared by the GNP method with G/N ratios of (a) 1.7 and (b) 1.5, and those of ZnO–$ZnCr_2O_4$ catalysts prepared by the GNP method with G/N ratios of (c) 1.7 and (d) 1.5, after SRM treatment.

catalytic reaction.[60] Based on the BET results, the specific surface areas of the as-combusted ZnO–$ZnCr_2O_4$ and $ZnCr_2O_4$ catalysts ranged from 29 m^2 g^{-1} to 46 m^2 g^{-1}, and the results of BET revealed a large S_{BET}. Furthermore, the surface areas of the ZnO–$ZnCr_2O_4$ and $ZnCr_2O_4$ catalysts decreased as the G/N ratio increased. Furthermore, the surface area of the activated $ZnCr_2O_4$ and ZnO–$ZnCr_2O_4$ (G/N = 1.7) catalyst was 27 m^2 g^{-1} and 48 m^2 g^{-1}, respectively. Compared to the ZnO–$ZnCr_2O_4$ catalyst with G/N ratios of 1.7 before and after the activation, the surface area was increased by more than about 30% which could correspond to the catalyst test result shown in Table 3 and Fig. 9.

3.2 Characteristics of ZnO–$ZnCr_2O_4$ composite catalyst and $ZnCr_2O_4$ catalyst after SRM treatment

Fig. 6 presents the X-ray diffraction patterns of $ZnCr_2O_4$ and ZnO–$ZnCr_2O_4$ prepared by the GNP method with G/N ratios of 1.5 and 1.7 after steam reforming treatment. As shown in the XRD patterns, the $ZnCr_2O_4$ and ZnO–$ZnCr_2O_4$ catalysts retained the cubic phase spinel structure of $ZnCr_2O_4$ (PDF# 87-0028) after the catalyst test, as revealed by Fig. 6(a–d). Moreover, after the SRM treatment, the crystallinity of the ZnO phase in the ZnO–$ZnCr_2O_4$ composite catalyst was significantly improved. This indicated that the ZnO particles attached to the surface of the catalyst experienced grain growth during the SRM process, as shown in Fig. 6(c) and (d).

SEM images of the $ZnCr_2O_4$ and ZnO–$ZnCr_2O_4$ (G/N ratio 1.5 and 1.7) catalysts after steam reforming treatment are presented in Fig. 7. As can be seen in the figure, they still retained the porous structure produced in the GNP process. Because of the gas product generated during the reaction of SRM, the porous structure of $ZnCr_2O_4$ and ZnO–$ZnCr_2O_4$ catalyst was retained, as shown in Fig. 7(a–d). It can be seen from the SEM images in

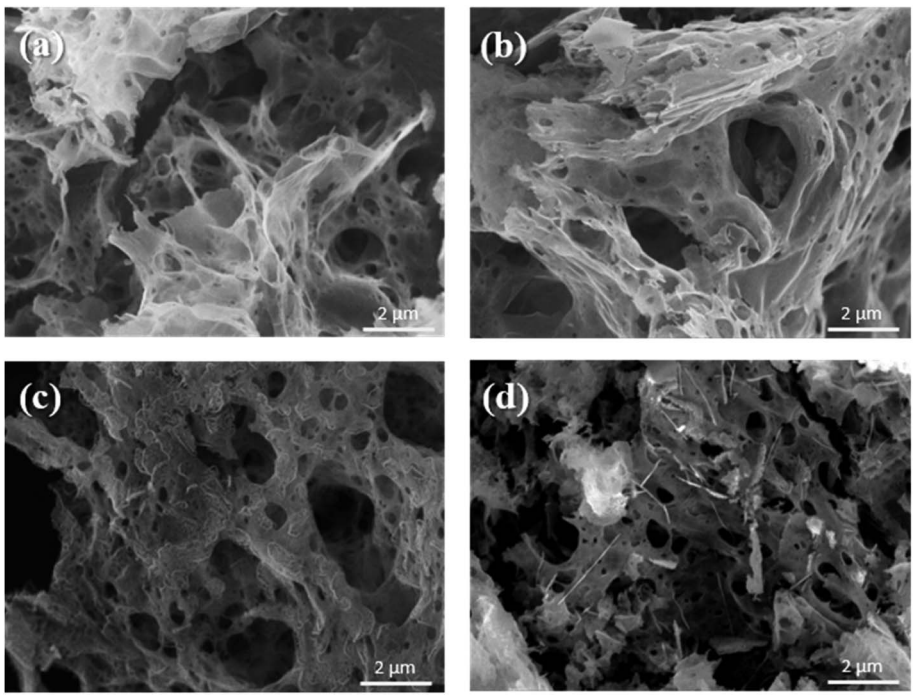

Fig. 7 SEM images of $ZnCr_2O_4$ catalysts prepared by the GNP method with G/N ratios of (a) 1.7 and (b) 1.5, and those of ZnO–$ZnCr_2O_4$ catalysts prepared by the GNP method with G/N ratios of (c) 1.7 and (d) 1.5, after SRM treatment.

Table 2 H_2 production rates of $ZnO–ZnCr_2O_4$ and $ZnCr_2O_4$ catalysts were prepared by the GNP method at different temperatures with a N_2 flow rate of 30 sccm

Rate of H_2 production (ml STP min^{-1} $g\text{-}cat^{-1}$)				
Composition	350 °C	400 °C	450 °C	500 °C
$ZnCr_2O_4$ G/N-1.7	1714	2700	3549	2410
$ZnCr_2O_4$ G/N-1.5	2453	2753	4122	4402
$ZnO–ZnCr_2O_4$ G/N-1.7	1286	3046	4814	3954
$ZnO–ZnCr_2O_4$ G/N-1.5	1860	2573	4074	2663

Fig. 7(c) and (d) that the addition of ZnO to the $ZnCr_2O_4$ catalyst increased the number of active sites and contributed to hydrogen production in the SRM process.

For the catalyst test in this study, the $ZnCr_2O_4$ and $ZnO–ZnCr_2O_4$ catalysts prepared under different conditions were evaluated according to the hydrogen production rate (ml STP min^{-1} $g\text{-}cat^{-1}$), and the efficiencies of the $ZnCr_2O_4$ and $ZnO–ZnCr_2O_4$ catalysts with and without activation were also compared. The H_2 production rate was estimated with a gas chromatograph equipped with TCD. The catalyst was placed in the reaction bed for the SRM process at temperatures of 350 °C to 500 °C, and then the reacted gas was assisted by the N_2 at a flow rate of 30 sccm. The catalyst was thermally treated at the reaction temperature prior to the reaction without contact with methanol vapor to maximize the hydrogen conversion capacity and the life of the catalyst.[47]

The hydrogen production rates of the $ZnCr_2O_4$ and $ZnO–ZnCr_2O_4$ catalysts prepared with different G/N ratios at reaction temperatures of 350 °C to 500 °C are listed in Table 2. The H_2 production rates of the $ZnCr_2O_4$ and $ZnO–ZnCr_2O_4$ catalysts are illustrated in Fig. 8. It can be seen that, when the reaction temperature rose, the hydrogen production performance of the catalyst increased. The $ZnO–ZnCr_2O_4$ G/N-1.7 composite catalyst had the best hydrogen production efficiency when the gas product was carried by N_2, the N_2 flow rate was 30 sccm, and the temperature was 450 °C. The hydrogen production rate of the $ZnO–ZnCr_2O_4$ G/N-1.7 composite catalyst was estimated at 4814.25 ml STP min^{-1} $g\text{-}cat^{-1}$. According to this result, the catalytic performance improved when the optimum catalyst reaction temperature decreased after the addition of ZnO. Zhang *et al.* reported that the incorporation of ZnO could affect the hydrogen production rate and that a suitable amount of ZnO content in the catalyst modified the active site on the surface and limited the agglomeration of the particles.[61] Moreover, H_2 production enhancement by the ZnO incorporation into $ZnCr_2O_4$ which was binary crystal structure $ZnO–ZnCr_2O_4$ formed with a close connection of hexagonal ZnO and $ZnCr_2O_4$ phases and it was helpful to improve the interaction between ZnO and $ZnCr_2O_4$. Xiaofeng *et al.* reported the morphology and facet of ZnO played an important role in affecting its catalytic activity. Several studies have reported that the terminal polar (0001) facets were more active surfaces for catalysis than the nonpolar surfaces perpendicular to them.[62]

A high hydrogen production rate is essential for the realization of fuel cells for automotive and mobile applications. However, hydrogen production reactors are generally dangerous due to flammability and explosion hazards. However, the $ZnO–ZnCr_2O_4$ composite catalyst can be used directly without high-temperature activation, and it is extremely stable. Therefore, the catalyst in this study would be useful in vehicles with fuel cells because of its simple hydrogen production by SRM and its high efficiency.

Furthermore, the hydrogen production rates of the activated catalysts were also respectively investigated. The $ZnO–ZnCr_2O_4$ and $ZnCr_2O_4$ catalysts were activated in a mixture of 10% H_2 and 90% N_2 gas at 650 °C for 1 hour before the SRM process. The results of the catalyst tests are listed in Table 3 and illustrated in Fig. 9. According to the results, the optimal reaction temperature of $ZnO–ZnCr_2O_4$ composite increased to 500 °C. However, the optimal reaction temperature was increased because of the thermal treatment during the activation. Liyan *et al.* reported that $ZnO–ZnCr_2O_4$ composite treated with various thermal treatments revealed a reduction shift to the higher temperature in thermal treatment, indicating the synergetic effect shown by ZnO and $ZnCr_2O_4$.[48] The activated $ZnO–ZnCr_2O_4$ G/N-1.7 had the best hydrogen production rate, which reached 6299 ml STP min^{-1} $g\text{-}cat^{-1}$. The activated $ZnO–ZnCr_2O_4$ composite

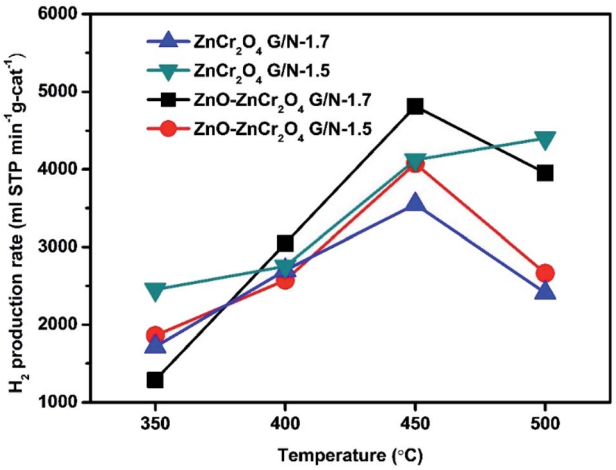

Fig. 8 The H_2 production rates of $ZnO–ZnCr_2O_4$ and $ZnCr_2O_4$ catalysts prepared by the GNP method at different temperatures with a N_2 flow rate of 30 sccm.

Table 3 H_2 production rates of activated $ZnO–ZnCr_2O_4$ and $ZnCr_2O_4$ catalysts (G/N-1.7) at different temperatures with a N_2 flow rate of 30 sccm

Rate of H_2 production (ml STP min^{-1} $g\text{-}cat^{-1}$)		
Reactor temperature	$ZnO–ZnCr_2O_4$ G/N-1.7 (activated)	$ZnCr_2O_4$ G/N-1.7 (activated)
350 °C	1681	1035
400 °C	2467	2272
450 °C	4185	3896
500 °C	6299	5865
550 °C	4503	3571

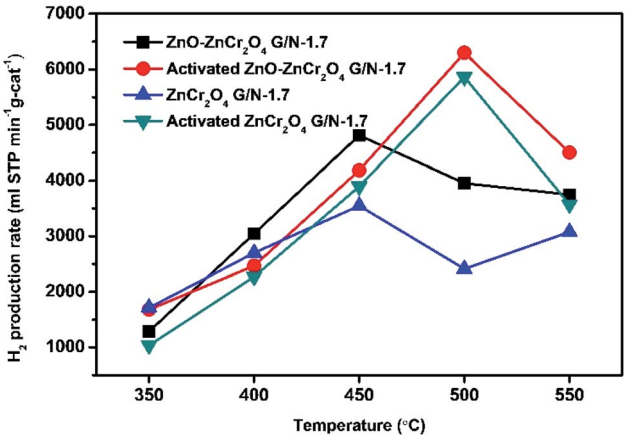

Fig. 9 H_2 production rates of activated ZnO–$ZnCr_2O_4$ and $ZnCr_2O_4$ catalysts (G/N-1.7) at different temperatures with a N_2 flow rate of 30 sccm.

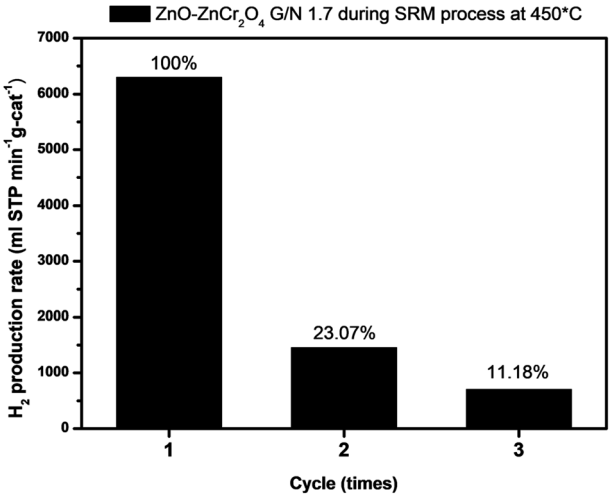

Fig. 11 The cycle test study of ZnO–$ZnCr_2O_4$ catalyst (G/N-1.7) during SRM at 450 °C with a N_2 flow rate of 30 sccm.

catalyst also had higher activity and hydrogen production than those of the inactivated ZnO–$ZnCr_2O_4$ composite catalyst.

Fig. 10 compares the hydrogen production rates of ZnO–$ZnCr_2O_4$ and $ZnCr_2O_4$ powders prepared by GNP (with and without activation); a commercial catalyst;[24] $CuCrO_2$ bulk powder,[26] $CuCrO_2$, $CuFeO_2$, and $CuFeO_2$–CeO_2 nanopowders prepared by GNP.[8,14] The results show that the catalytic performance in hydrogen production reported in this study was higher than those of the aforementioned catalysts. Furthermore, the stability and the cycle-life were studied. Furthermore, the stability and the cycle-life were studied. In addition, to investigate the reusability of the ZnO–$ZnCr_2O_4$ composite catalyst, Fig. 11 was shown ZnO–$ZnCr_2O_4$ composite catalyst activity of changes with repeated cycle test during the SRM process which reacted at 450 °C with an N_2 flow rate of 30 sccm. ZnO–$ZnCr_2O_4$ composite after 3 times SRM treatment, the H_2 production rates of the ZnO–$ZnCr_2O_4$ composite G/N-1.7 decreased by about 90%.

Based on the characteristics of the ZnO–$ZnCr_2O_4$ composite catalyst and $ZnCr_2O_4$ catalyst after SRM treatment, the ZnO–$ZnCr_2O_4$ and $ZnCr_2O_4$ catalysts prepared by the GNP method showed a reasonable degree of stability and exhibited better catalytic efficiency than those of the previous copper-based catalyst. The appropriate incorporation of ZnO in the ZnO–$ZnCr_2O_4$ catalyst increased the active sites and contributed to the hydrogen production function.

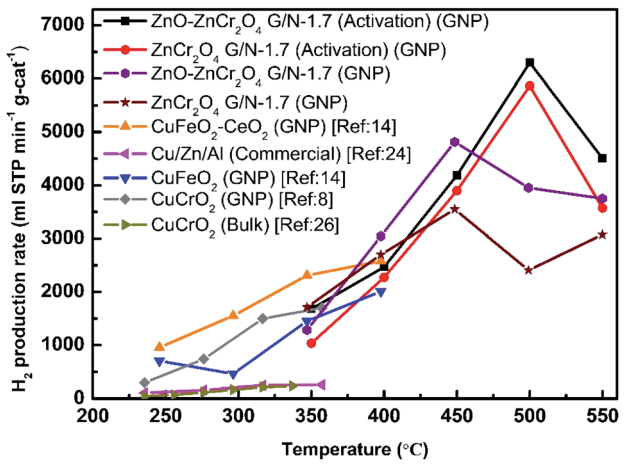

Fig. 10 The H_2 production rates in SRM of the ZnO–$ZnCr_2O_4$ and $ZnCr_2O_4$ powders prepared by GNP with and without the activation inflow rate of 30 sccm, and the H_2 production rates of a commercial catalyst,[24] $CuCrO_2$ bulk powder,[26] and the $CuCrO_2$, $CuFeO_2$, and $CuFeO_2$–CeO_2 nanopowders prepared by GNP.[8,14]

4. Conclusions

A zinc-based catalyst, namely, ZnO–$ZnCr_2O_4$ porous composite was prepared by GNP with G/N ratios of 1.7 and 1.5. The catalysts prepared in this study were applied to hydrogen production by SRM. The ZnO–$ZnCr_2O_4$ porous composite catalysts, before activation pretreatment, exhibited superior catalytic performance in the SRM process as compared with the previous copper-based catalyst and a commercial catalyst. Without activation pretreatment, the ZnO–$ZnCr_2O_4$ porous composite catalyst made with a G/N ratio of 1.7 revealed the best hydrogen production rate, 4814 ml STP min^{-1} $g\text{-}cat^{-1}$, at a reaction temperature of 450 °C and N_2 flow rate of 30 sccm. After activation, the ZnO–$ZnCr_2O_4$ porous composite catalyst exhibited hydrogen production of 6299 ml STP min^{-1} $g\text{-}cat^{-1}$ at 500 °C and a N_2 flow rate of 30 sccm. Furthermore, to investigate the characteristics of the catalyst prepared by GNP and the catalyst after the SRM process, the ZnO–$ZnCr_2O_4$ porous composite catalysts were analyzed by XRD, FE-SEM, and BET. The catalytic performance was determined by GC-TCD. Due to the GNP process, the catalyst had a porous structure, which effectively increased the specific surface area and thus the catalytic activity. The ZnO–$ZnCr_2O_4$ porous composite catalyst features a simple process with good performance for hydrogen production from SRM. The advantages of the ZnO–$ZnCr_2O_4$ composite

catalyst make it a potential material for fuel cells in automobiles.

Conflicts of interest

The authors declare that they have no known competing financial interests or personal relationships that could have appeared to influence the work reported in this paper.

Acknowledgements

This work was supported by the Ministry of Science and Technology of Taiwan (MOST 108-2221-E-027-056, MOST 109-2221-E-027-068, MOST 109-2221-E-027-059, and MOST 109-2113-M-027-001-MY3). This work was supported by the National Science and Technology Council of Taiwan (NSTC 111-2221-E-027-104). This work was supported by University System of Taipei Joint Research Program (USTP-NTUT-TMU-111-01). The authors appreciate the Precision Research and Analysis Centre of National Taipei University of Technology (NTUT) for providing the measurement facilities.

References

1 N. Armaroli and V. Balzani, The future of energy supply: Challenges and opportunities, *Angew. Chem., Int. Ed.*, 2007, **46**, 52–66.

2 C. Pojanavaraphan, A. Luengnaruemitchai and E. Gulari, Hydrogen production by oxidative steam reforming of methanol over Au/CeO_2 catalysts, *Chem. Eng. J.*, 2012, **192**, 105–113.

3 V. Shanmugam, S. Neuberg, R. Zapf, H. Pennemann and G. Kolb, Hydrogen production over highly active Pt based catalyst coatings by steam reforming of methanol: Effect of support and co-support, *Int. J. Hydrogen Energy*, 2019, **45**, 1658–1670.

4 N. Edwards, S. R. Ellis, J. C. Frost, S. E. Golunski, A. N. J. V. Keulen, N. G. Lindewald and J. G. Reinkingh, On-board hydrogen generation for transport applications: The HotSpotTM methanol processor, *J. Power Sources*, 1998, **71**, 123–128.

5 C. Song, Fuel processing for low-temperature and high-temperature fuel cells: Challenges, and opportunities for sustainable development in the 21st century, *Catal. Today*, 2002, **77**, 17–49.

6 M. A. K. Lodhi and R. W. Mires, How safe is the storage of liquid hydrogen ?, *Int. J. Hydrogen Energy*, 1989, **14**, 35–43.

7 T. W. Chiu and Y. S. Lu, Preparation of $CuCr_{1-x}Fe_xO_2$ delafossite solid solution powder *via* a self-combustion glycine nitrate process, *Ferroelectrics*, 2016, **491**, 149–154.

8 T. W. Chiu, R. T. Hong, B. S. Yu, Y. H. Huang, S. Kameoka and A. P. Tsai, Improving steam-reforming performance by nanopowdering $CuCrO_2$, *Int. J. Hydrogen Energy*, 2014, **39**, 14222–14226.

9 S. Schuyten and E. E. Wolf, Selective combinatorial studies on Ce and Zr promoted Cu/Zn/Pd catalysts for hydrogen production *via* methanol oxidative reforming, *Catal. Lett.*, 2006, **106**, 7–14.

10 S. F. Wang, C. M. Lu, Y. C. Wu, Y. C. Yang and T. W. Chiu, La_2O_3-Al_2O_3-B_2O_3-SiO_2 glasses for solid oxide fuel cell applications, *Int. J. Hydrogen Energy*, 2011, **36**, 3666–3672.

11 H. Ji, J. Lee, E. Choi and I. Seo, Hydrogen production from steam reforming using an indirect heating method, *Int. J. Hydrogen Energy*, 2018, **43**, 3655–3663.

12 M. Turco, G. Bagnasco, U. Costantino, F. Marmottini, T. Montanari, G. Ramis and G. Busca, Production of hydrogen from oxidative steam reforming of methanol: I. Preparation and characterization of Cu/ZnO/Al_2O_3 catalysts from a hydrotalcite-like LDH precursor, *J. Catal.*, 2004, **228**, 43–45.

13 D. R. Palo, R. A. Dagle and J. D. Holladay, Methanol steam reforming for hydrogen production, *Chem. Rev.*, 2007, **107**, 3992–4021.

14 C. L. Yu, S. Sakthinathan, B. Y. Hwang, S. Y. Lin, T. W. Chiu, B. S. Yu, Y. J. Fan and C. Chuang, $CuFeO_2$–CeO_2 nanopowder catalyst prepared by self-combustion glycine nitrate process and applied for hydrogen production from methanol steam reforming, *Int. J. Hydrogen Energy*, 2020, **45**, 15752–15762.

15 J. D. Holladay, Y. Wang and E. Jones, Review of developments in portable hydrogen production using microreactor technology, *Chem. Rev.*, 2004, **104**, 4767–4789.

16 S. Velu, K. Suzuki, M. P. Kapoor, F. Ohashi and T. Osaki, Selective production of hydrogen for fuel cells *via* oxidative steam reforming of methanol over CuZnAl(Zr)-oxide catalysts, *Appl. Catal., A*, 2001, **213**, 47–63.

17 T. Shishido, Y. Yamamoto, H. Morioka and K. Takehira, Production of hydrogen from methanol over Cu/ZnO and Cu/ZnO/Al_2O_3 catalysts prepared by homogeneous precipitation: Steam reforming and oxidative steam reforming, *J. Mol. Catal. A: Chem.*, 2007, **268**, 185–194.

18 C. M. Kalamaras and A. M. Efstathiou, *Hydrogen Production Technologies: Current State and Future Developments*, Conf Pap Energy, 2013, pp. 1–9.

19 H. S. Pajaie, Hydrogen Production from Methanol Steam Reforming over Cu/ZnO/Al2O_3/CeO_2/ZrO_2 Nanocatalyst in an Adiabatic Fixed-Bed Reactor, *Iran. J. Energy Environ.*, 2012, **3**, 307–313.

20 J. Papavasiliou, G. Avgouropoulos and T. Ioannides, Production of hydrogen *via* combined steam reforming of methanol over CuO-CeO_2 catalysts, *Catal. Commun.*, 2004, **5**, 231–235.

21 J. C. Brown and E. Gulari, Hydrogen production from methanol decomposition over Pt/Al_2O_3 and ceria promoted Pt//Al_2O_3 catalysts, *Catal. Commun.*, 2004, **5**, 431–436.

22 M. G. Poirier and C. Sapundzhiev, Catalytic decomposition of natural gas to hydrogen for fuel cell applications, *Int. J. Hydrogen Energy*, 1997, **22**, 429–433.

23 J. Agrell, K. Hasselbo, K. Jansson, S. G. Jaras and M. Boutonnet, Production of hydrogen by partial oxidation of methanol over Cu/ZnO catalysts prepared by microemulsion technique, *Appl. Catal., A*, 2001, **211**, 239–250.

24 S. Kameoka, T. Tanabe and A. P. Tsai, Self-assembled porous nano-composite with high catalytic performance by reduction of tetragonal spinel $CuFe_2O_4$, *Appl. Catal., A*, 2010, **375**, 163–171.

25 R. P. Hernandez, G. M. Galicia, D. M. Anaya, J. Palacios, C. A. Chavez and J. A. Alatorre, Synthesis and characterization of bimetallic Cu-Ni/ZrO_2 nanocatalysts: H_2 production by oxidative steam reforming of methanol, *Int. J. Hydrogen Energy*, 2008, **33**, 4569–4576.

26 S. Kameoka, M. Okada and A. P. Tsai, Preparation of a novel copper catalyst in terms of the immiscible interaction between copper and chromium, *Catal. Lett.*, 2008, **120**, 252–256.

27 T. L. Reitz, S. Ahmed, M. Krumpelt, R. Kumar and H. H. Kung, Characterization of CuO/ZnO under oxidizing conditions for the oxidative methanol reforming reaction, *J. Mol. Catal. A: Chem.*, 2000, **162**, 275–285.

28 M. V. Twigg and M. S. Spencer, Deactivation of supported copper metal catalysts for hydrogenation reactions, *Appl. Catal., A*, 2001, **212**, 161–174.

29 N. Liu, Z. Yuan, S. Wang, C. Zhang, S. Wang and D. Li, Characterization and performance of a ZnO-$ZnCr_2O_4$/CeO_2-ZrO_2 monolithic catalyst for methanol auto-thermal reforming process, *Int. J. Hydrogen Energy*, 2008, **33**, 1643–1651.

30 S. Chandrasekaran, D. Ma, Y. Ge, L. Deng, C. Bowen, J. Roscow, Y. Zhang, Z. Lin, R. D. K. Misra, J. Li, P. Zhang and H. Zhang, Electronic structure engineering on two-dimensional (2D) electrocatalytic materials for oxygen reduction, oxygen evolution, and hydrogen evolution reactions, *Nano Energy*, 2020, **77**, 105080.

31 S. Chandrasekaran, L. Yao, L. Deng, C. Bowen, Y. Zhang, S. Chen, Z. Lin, F. Peng and P. Zhang, Recent advances in metal sulfides: from controlled fabrication to electrocatalytic, photocatalytic and photoelectrochemical water splitting and beyond, *Chem. Soc. Rev.*, 2019, **48**, 4178–4280.

32 R. Kalia, Pushpendra, R. K. Kunchala, S. N. Achary and B. S. Naidu, New insights on photocatalytic hydrogen evolution of $ZnFe_{2-x}Ga_xO_4$ ($0 \leq x \leq 2$) solid solutions: Role of oxygen vacancy and ZnO segregated phase, *J. Alloys Compd.*, 2021, **875**, 159905.

33 Y. F. Li, X. F. Dong and W. M. Lin, Effects of ZrO_2-promoter on catalytic performance of CuZnAlO catalysts for production of hydrogen by steam reforming of methanol, *Int. J. Hydrogen Energy*, 2004, **29**, 1617–1621.

34 P. H. Matter, D. J. Braden and U. S. Ozkan, Steam reforming of methanol to H_2 over nonreduced Zr-containing CuO/ZnO catalysts, *J. Catal.*, 2004, **223**, 340–351.

35 B. Lindström, L. J. Pettersson and G. Menon, Activity and characterization of Cu/Zn, Cu/Cr and Cu/Zr on γ-alumina for methanol reforming for fuel cell vehicles, *Appl. Catal., A*, 2002, **234**, 111–125.

36 W. Tong, A. West, K. Cheung, K. M. Yu and S. C. E. Tsang, Dramatic effects of gallium promotion on methanol steam reforming Cu-ZnO catalyst for hydrogen production: Formation of 5Å copper clusters from Cu-$ZnGaO_x$, *ACS Catal.*, 2013, **3**, 1231–1244.

37 S. Chandrasekaran, C. Zhang, Y. Shu, H. Wang, S. Chen, T. Nesakumar Jebakumar Immanuel Edison, Y. Liu, N. Karthik, R. D. K. Misra, L. Deng, P. Yin, Y. Ge, O. A. A. Hartomy, A. A. Ghamdi, S. Wageh, P. Zhang, C. Bowen and Z. Han, Advanced opportunities and insights on the influence of nitrogen incorporation on the physico-/electro-chemical properties of robust electrocatalysts for electrocatalytic energy conversion, *Coord. Chem. Rev.*, 2021, **449**, 214209.

38 S. Chandrasekaran, M. Khandelwal, F. Dayong, L. Sui, J. S. Chung, R. D. K. Misra, P. Yin, E. J. Kim, W. Kim, A. Vanchiappan, Y. Liu, S. H. Hur, H. Zhang and C. Bowen, Developments and perspectives on robust nano-and microstructured binder-free electrodes for bifunctional water electrolysis and beyond, *Adv. Energy Mater.*, 2022, **12**, 2200409.

39 L. A. Ying, J. Liu, L. Mo, H. Lou and X. Zheng, Hydrogen production by oxidative steam reforming of methanol over $Ce_{1-x}Zn_xO_y$ catalysts prepared by combustion method, *Int. J. Hydrogen Energy*, 2012, **37**, 1002–1006.

40 S. Y. Lin, T. W. Chiu and C. Dong, Preparation and characterization of $CuCrO_2$-CeO_2 composite nanopowder by a self-combustion glycine nitrate process, *Ceram. Int.*, 2017, **43**, S639–S642.

41 S. Dey, B. S. Naidu and C. N. R. Rao, $Ln_{0.5}A_{0.5}MnO_3$ (Ln = Lanthanide, A = Ca, Sr) Perovskites exhibiting remarkable performance in the thermochemical generation of CO and H_2 from CO_2 and H_2O, *Chem. – Eur. J.*, 2015, **21**, 7077–7081.

42 S. Dey, B. S. Naidu and C. N. R. Rao, Beneficial effects of substituting trivalent ions in the B-site of $La_{0.5}Sr_{0.5}Mn_{1-x}A_xO_3$ (A = Al, Ga, Sc) on the thermochemical generation of CO and H_2 from CO_2 and H_2O, *Dalton Trans.*, 2016, **45**, 2430–2435.

43 S. Dey, B. S. Naidu, A. Govindaraj and C. N. R. Rao, Noteworthy performance of $La_{1-x}Ca_xMnO_3$ perovskites in generating H_2 and CO by the thermochemical splitting of H_2O and CO_2, *Phys. Chem. Chem. Phys.*, 2015, **17**, 122–125.

44 A. G. Merzhanov, Combustion and explosion processes in physical chemistry and technology of inorganic materials, *Russ. Chem. Rev.*, 2003, **72**, 323–345.

45 L. A. Chick, L. R. Pederson, G. D. Maupin, J. L. Bates, L. E. Thomas and G. J. Exarhos, Glycine-nitrate combustion synthesis of oxide ceramic powders, *Mater. Lett.*, 1990, **10**, 6–12.

46 T. W. Chiu and P. S. Huang, Preparation of delafossite $CuFeO_2$ coral-like powder using a self-combustion glycine nitrate process, *Ceram. Int.*, 2013, **39**, S575–S578.

47 B. Y. Hwang, S. Sakthinathan and T. W. Chiu, Production of hydrogen from steam reforming of methanol carried out by self-combusted $CuCr_{1-x}Fe_xO_2$ (x = 0_1) nanopowders catalyst, *Int. J. Hydrogen Energy*, 2019, **44**, 2848–2856.

48 L. Wang, X. Gao, Y. Bai, M. Tan, K. Suna, T. Zhang, Y. Wu, J. Pan, H. Xie and Y. Tana, The synergistic effect between ZnO and $ZnCr_2O_4$ on the catalytic performance for

isobutanol synthesis from syngas, *Fuel*, 2019, **253**, 1570–1577.

49 A. T. Baricevic, B. Grbic, D. Jovanovic, S. Angelov, D. Mehandziev, C. Marinova and P. K. Stefanov, Activity and sulphur tolerance of monophase spinels in carbon monoxide and C_xH_y oxidation, *Appl. Catal.*, 1989, **47**, 145–153.

50 E. Tronconi, L. Lietti, P. Forzatti and I. Pasquon, Higher Alcohol Synthesis over Alkali Metal-Promoted High-Temperature Methanol Catalysts, *Appl. Catal.*, 1989, **47**, 317–333.

51 A. Abbasi, M. Hamadanian, M. S. Niasari and S. M. Derazkola, Facile size-controlled preparation of highly photocatalytically active $ZnCr_2O_4$ and $ZnCr_2O_4$/Ag nanostructures for removal of organic contaminants, *J. Colloid Interface Sci.*, 2017, **500**, 276–284.

52 N. Liu, Z. Yuan, S. Wang, C. Zhang, S. Wang and D. Li, Characterization and performance of a ZnO- $ZnCr_2O_4$/CeO_2-ZrO_2 monolithic catalyst for methanol auto-thermal reforming process, *Int. J. Hydrogen Energy*, 2008, **33**, 1643–1651.

53 G. Drazic and M. Trontelj, Preparation and properties of ceramic sensor elements based on $MgCr_2O_4$, *Sens. Actuators*, 1989, **18**, 407–414.

54 S. A. Hosseini and M. C. A. Galvan, Study of physical-chemical properties and catalytic activities of $ZnCr_2O_4$ spinel nano oxides obtained from different methods-Modeling the synthesis process by response surface methodology and optimization by genetic algorithm, *J. Taiwan Inst. Chem. Eng.*, 2016, **61**, 261–269.

55 J. Nakamura, T. Fujitani, S. Kuld, S. Helveg, I. Chorkendorff and J. Sehested, Active sites for CO_2 hydrogenation to methanol on Cu/ZnO catalysts, *Science*, 2017, **357**, 1296–1299.

56 E. A. C. Miranda, J. F. M. Carvaja and O. J. R. Baena, Effect of the fuels glycine, urea and citric acid on synthesis of the ceramic pigment $ZnCr_2O_4$ by solution combustion, *Mater. Res.*, 2015, **18**, 1038–1043.

57 T. W. Chiu, B. S. Yu, Y. R. Wang, K. T. Chen and Y. T. Lin, Synthesis of nanosized $CuCrO_2$ porous powders *via* a self-combustion glycine nitrate process, *J. Alloys Compd.*, 2011, **509**, 2933–2935.

58 M. Taghizadeh, H. Akhoundzadeh, A. Rezayan and M. Sadeghian, Excellent catalytic performance of 3D-mesoporous KIT-6 supported Cu and Ce nanoparticles in methanol steam reforming, *Int. J. Hydrogen Energy*, 2018, **43**, 10926–10937.

59 A. Iulianelli, P. Ribeirinha, A. Mendes and A. Basile, Methanol steam reforming for hydrogen generation *via* conventional and membrane reactors: A review, *Renewable Sustainable Energy Rev.*, 2014, **29**, 355–368.

60 T. W. Chiu and Y. W. Feng, Preparation of $CuCrO_2$ powders with high surface areas, *Key Eng. Mater.*, 2014, **617**, 187–190.

61 G. Zhang, J. Zhao, T. Yang, Q. Zhang and L. Zhang, In-situ self-assembled Cu_2O/ZnO core-shell catalysts synergistically enhance the durability of methanol steam reforming, *Appl. Catal., A*, 2021, **616**, 118072.

62 X. Gao, T. Zhang, Y. Wu, G. Yang, M. Tan, X. Li, H. Xie, J. Pan and Y. Tan, Isobutanol synthesis from syngas on Zn-Cr based catalysts: New insights into the effect of morphology and facet of ZnO nanocrystal, *Fuel*, 2018, **217**, 21–30.